

Analysis of subsonic premixed turbulent reacting flow in a backward-step combustor using PaSR models

*Anna Shiryayeva**, *Alexey Troshin***, *Vladimir Vlasenko**** and *Vladimir Sabelnikov*****

**Central Aerohydrodynamic Institute, Zhukovsky, Russia*

anja.shiryayeva@gmail.com

***Central Aerohydrodynamic Institute, Zhukovsky, Russia*

Moscow Institute of Physics and Technology, Dolgoprudny, Russia

ai-troshin@yandex.ru

****Central Aerohydrodynamic Institute, Zhukovsky, Russia*

Moscow Institute of Physics and Technology, Dolgoprudny, Russia

vlasenko.vv@yandex.ru

*****Central Aerohydrodynamic Institute, Zhukovsky, Russia*

ONERA, Palaiseau, France

vladimir.sabelnikov@onera.fr

Abstract

An example of Partially Stirred Reactor (PaSR) models application within RANS framework to the description of flows with turbulent combustion is presented. P. Magre et al. experiment of a methane/air premixed combustion in a subsonic flow in duct with a reverse step is simulated numerically. The focus is on Turbulence/Combustion Interaction contribution, on the analysis of combustion stabilization mechanism and on arising in calculations oscillations study. Influence of turbulent transport coefficients is considered. The simulation results are compared with the experiment and with calculations by other authors. Preliminary results of LES calculations are presented.

1. Introduction

Turbulent combustion simulation is one of the least understood problems of fluid and gas mechanics. The description of turbulent flows without combustion has now achieved significant success. Many turbulence models have been developed to describe flows within the framework of Reynolds equations (RANS – Reynolds Averaged Navier – Stokes Equations). Great achievements have been made in direct numerical modeling of large-scale turbulence (LES – Large Eddy Simulation). But the problem of turbulent combustion is still far from a satisfactory solution – despite the fact that research in this field has been underway for almost 80 years (Damköler’s first theoretical work [1] was published in 1940).

This is largely due to the specifics of the problem, where the main role is not played by turbulent diffusion processes, which are played mainly at the level of large turbulent vortices, but by molecular mixing processes occurring at the level of the smallest turbulent structures close to the Kolmogorov scale. There is an acute problem of creating physical and mathematical models that correctly describe components mixing, heat diffusion, combustion ignition, stabilization and extinction. It is worth noting the importance of Turbulence/Combustion Interaction (TCI) correct description and the ambiguity in choosing the optimal approach for simulation of flows with heat release, especially for high-speed flows. Of particular difficulty are mixed combustion regimes, in which there are areas with different flame stabilization mechanisms. A detailed discussion of turbulent combustion problem can be found in books [2–6].

To date, various approaches for TCI account have been developed: statistical methods (the method of moments, probability density function method), microlaminar flames models (flamelet), and many others (see, for example, [2–7]). In current work different variants of Partially Stirred Reactor model (PaSR) are used. An example of the application of these models to description of turbulent combustion flows is presented – simulation of the P. Magre et al. [8] experiment on combustion of subsonic premixed methane/air mixture in a channel with a reverse step. The simulation results are compared with the experiment and calculations of other authors. The focus is on TCI contribution, on the analysis of combustion stabilization mechanism and on arising in calculations oscillations study.

2. Used models and methods

Numerical simulation of flows was carried out on the basis of the full system of Reynolds equations for unsteady three-dimensional turbulent flows (URANS) of a multicomponent viscous gas (a mixture of perfect gases) with non-equilibrium chemical reactions. A finite-volume 2nd order of accuracy numerical method [9] was used. An explicit Godunov–Kolgan scheme was used for convective fluxes, a central difference scheme for diffusive fluxes, and a local implicit approximation for the source terms. The equations are closed by a certain kinetics model and a differential turbulence model. q - ω Coakley turbulence model with compressibility corrections and a transition function for coefficients switch between the near-wall and free-turbulence regions [10] is used.

Two approaches were used to calculate the time-averaged chemical reaction rates. In the first approach, TCI was not taken into account, and the reaction rate was calculated by the usual Arrhenius formulas, into which the average flow parameters are substituted. Below this approach will be called “without TCI account”.

In the second approach, Partially Stirred Reactor models (PaSR) are used. In these models, it is assumed that at large Reynolds numbers, molecular mixing, heat transport, and chemical reactions occur mainly in the so-called “thin structures”, associated with the smallest turbulent vortices. These structures are considered as homogeneous reactors, where the reaction proceeds continuously. Molecular diffusion supplies fresh mixture to the thin structures from surrounding space, and also removes the reaction products from them. In addition, because of molecular diffusion, heat transport occurs between the thin structures and surrounding space. The main parameters of the model are fine structures volume fraction γ^* and characteristic residence time of gas in the reactor τ^* .

The basic variant of PaSR model is taken from [11]. It is based on the assumption that the reaction time in thin structures is much shorter than the characteristic time of the average flow. Then the state in thin structures is quasi-stationary and is described by an algebraic system of equations:

$$h^* = h^0, \quad \frac{S_i^*}{\rho^*} = \frac{Y_i^* - Y_i^0}{\tau^*},$$

where subscript * corresponds to thin structures, 0 – to surrounding space; ρ - density, Y_i is mass fraction of i^{th} component; $h^* \equiv \sum_i Y_i^* h_i(T^*)$ is enthalpy of mixture (enthalpies of separate components, $h_i(T)$, include the chemical energy); $S_i^* \equiv -m_i \sum_k \nu_{ik} W_k^*$ is the source term in equation Y_i^* ; m_i is molecular weight of i^{th} component; $W_k(T, \vec{Y}, \rho)$ is speed of k^{th} reaction [mole/(m³·s)]; ν_{ik} is stoichiometric coefficient in the equation of k^{th} reaction. $f^0 = h^0; Y_i^0$ are gas parameters in the space, surrounding the thin structures:

$$f^0 = \frac{\bar{\rho} \bar{f} - \gamma^* \rho^* f^*}{\bar{\rho} - \gamma^* \rho^*}.$$

Basic parameters of the model, γ^* and τ^* , are expressed as follows [12]:

$$\gamma^* = \frac{\tau_{chem}}{\tau_{chem} + \tau^*}; \quad \tau^* = \sqrt{\tau_K \cdot \tau_T} \quad (1)$$

where $\tau_K \approx \sqrt{\nu/\varepsilon}$ is Kolmogorov scale, $\tau_T \approx 1/\omega$ is turbulence macroscale (ν, ε, ω – kinematic viscosity, average turbulent energy dissipation rate and characteristic frequency of turbulent fluctuations), and τ_{chem} is characteristic time scale of chemical processes. It is usually assumed that $\tau_{chem} \approx \delta_L/S_L$, where S_L and $\delta_L \approx \nu/S_L$ are respectively characteristic speed and thickness of a laminar flame front.

In [13] the “Extended PaSR Model” (EPaSR) was proposed. In this model the parameters in thin structures (temperature and mass fractions of components) are described by a system of partial differential equations, taking into account the variation of thin structures in time and their transport in space:

$$\frac{\partial(\gamma^* \rho^* E^*)}{\partial t} + \frac{\partial}{\partial x_j} \left[\gamma^* \rho^* \left(E^* \bar{u}_j + \bar{p} \bar{u}_j + \tau_{mj} \bar{u}_m + q_j^* + \sum_{i=1}^{N_{sp}} h_j^* J_{ij}^* \right) \right] = -10.5 \omega \rho^* (h^* - h^0) + h^0 \frac{\dot{m} + |\dot{m}|}{2} + h^* \frac{\dot{m} - |\dot{m}|}{2}, \quad (2)$$

$$\frac{\partial(\gamma^* \rho^* Y_i^*)}{\partial t} + \frac{\partial}{\partial x_j} \left[\gamma^* \rho^* (Y_i^* \bar{u}_j + J_{ij}^*) \right] = \gamma^* S_i^* - 10.5 \omega \rho^* (Y_i^* - Y_i^0) + Y_i^0 \frac{\dot{m} + |\dot{m}|}{2} + Y_i^* \frac{\dot{m} - |\dot{m}|}{2}.$$

Here $E^* = \bar{u}_m \bar{u}_m / 2 + k + e^*$ is total energy per unit mass (k is kinetic energy of turbulence); τ_{mj} is summary diffusive flux of momentum (sum of viscous and turbulent stresses); q_j^* is summary diffusive flux of heat due to gradients of temperature T^* ; J_{ij}^* is summary diffusive flux of mass of i^{th} component; due to gradients of Y_i^* . Parameter τ^* is calculated through the second formula in (1), and γ^* is found from the following equation:

$$\frac{\partial(\gamma^* \rho^*)}{\partial t} + \frac{\partial}{\partial x_j} \left[\gamma^* \rho^* \bar{u}_j \right] = \dot{m}, \quad \dot{m} = -\rho^* \frac{\gamma^* - \gamma_{eq}^*}{\tau^*},$$

where γ_{eq}^* is calculated through the first formula in (1). Additional terms in Eq. (2), depending on \dot{m} , are related to mass transition from the surrounding space into thin structures and back. Once the characteristics of thin structures are determined, source terms in equations for average mass fractions \bar{Y}_i are calculated as $\bar{S}_i = \gamma^* S_i^*$.

3. Experiment by P. Magre et al. and its numerical simulation

P. Magre et al. experiment (ONERA) [8] is devoted to the study of subsonic premixed combustion of methane-air mixture, heated by an electric heater, in a duct of constant width 0.1 m with a backward-facing step – see fig. 1. A homogeneous in composition fuel/oxidant mixture with an equivalence ratio being equal to 0.8 arrives at the channel with the inflow velocity $u \sim 50$ m/s and temperature $T \sim 525$ K (Mach number $M \sim 0.1$). The turbulent fluctuations level, measured at a distance 0.15 m upstream from the step, was 11% of the average flow velocity in the experiment.

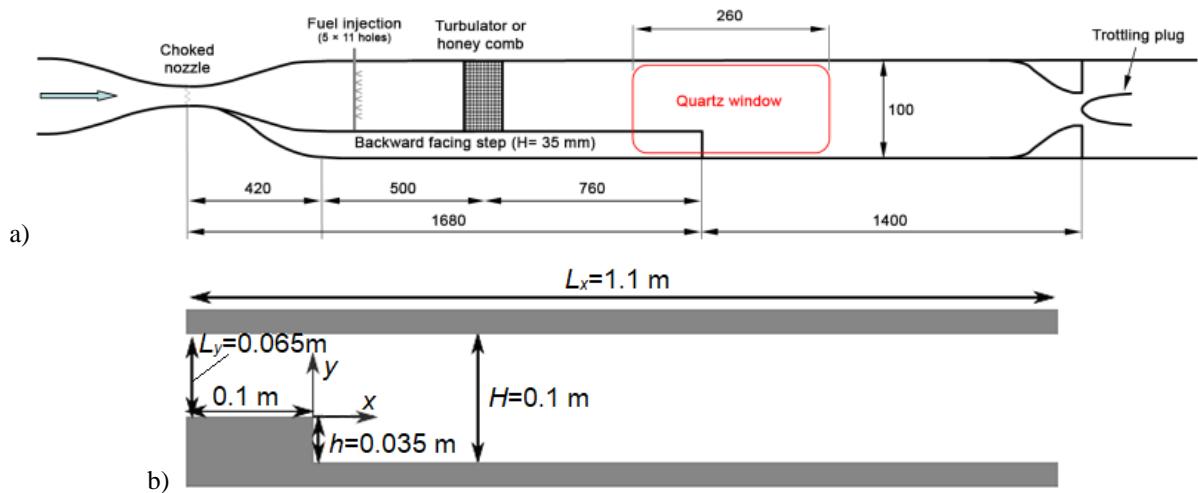


Figure 1. P. Magre et al. experiment [8]: a) scheme of A3C test bench along with optimal diagnostics and b) backward-facing step dimensions

In the experiments, the temperature and velocity profiles were measured by non-intrusive techniques (CARS and LDA). Numerical simulation of this experiment within the framework of two-dimensional RANS equations, closed by the $k-l$ turbulence model, is described in details in [12], both without accounting for TCI and with EPaSR model.

In the present work, the RANS calculations were performed also in 2D flow approximation (the grid contained one large cell in the 3^d lateral direction). The flow profiles in the inlet section were obtained from the numerical simulation of the flow in the duct upstream from the inlet. Herewith the values of velocity $u=58$ m/s and turbulent parameters $q\sim 7.5$ m/s, $\omega\sim 67.5$ Hz were obtained in an inviscid core of the flow. A constant pressure $p=1$ bar was set at the right border of the main duct. In the output and input sections, soft boundary conditions were applied, based on the analysis of Riemann invariants. In the experiment, the walls were cooled, but the temperature of the walls was not measured. So, as well as in the calculation work [12], the duct walls were assumed to be heat insulated.

On the basis of a series of calculations without reactions on several nested meshes, a coarse one was chosen, for which the influence of mesh resolution on the solution could be neglected. This coarse mesh (see fig. 2) was used for the first calculations with combustion. It contained a total amount of 13 311 cells, 38 cells for the step height, 36 cells across the main flow and 167 cells along length of the chamber from the step. Minimum cells size near the step and near the upper wall was $\Delta x\sim 1.16\times 10^{-3}$ m and $\Delta y\sim 6.4\times 10^{-4}$ m, accordingly.

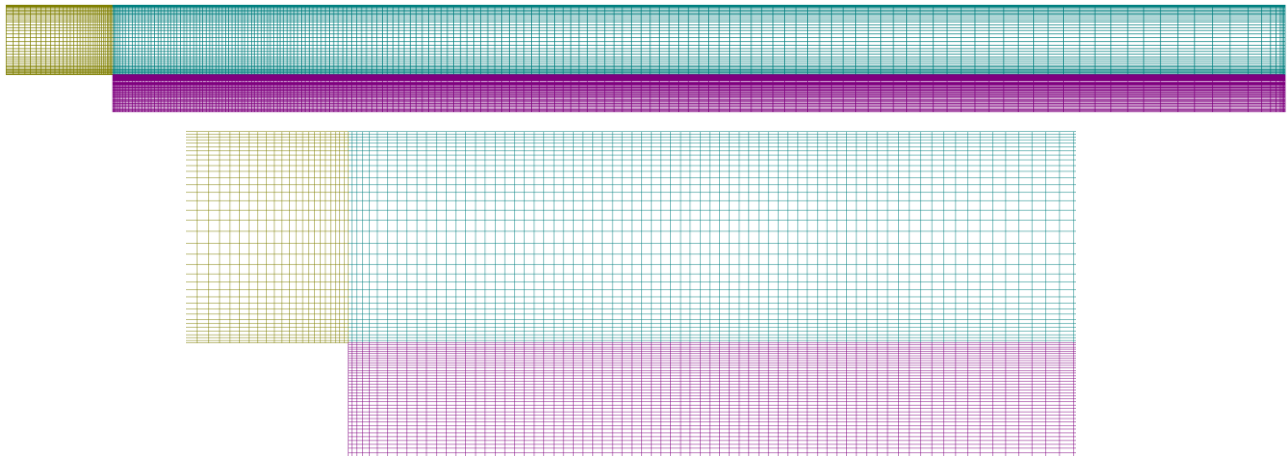


Figure 2: P. Magre et al. [8] experiment modeling: coarse mesh (general view and mesh in the step vicinity)

In this task, the wave mechanism of flame propagation due to thermal conductivity plays an important role. Therefore, the kinetic scheme of methane combustion in air, recommended in [14], was used. To initialize the combustion process, a high temperature and combustion products were set in the initial field. The flow development was resulted in formation of a quasi-periodic regime with weak fluctuations of parameters (about 1%). The flow fields were averaged over the oscillation period in order to be compared with the experimental data.

3.1 PaSR models application

In fig. 3 the temperature fields obtained in three calculations are compared: without TCI account and based on the PaSR and EPaSR models. TCI account changes significantly the flow pattern. The PaSR model, which does not take into account the fine structures transport over space, has generated a nonphysical S-shaped flame structure near the step. In the case of EPaSR model, this defect is carried down by the flow.

Fields of the fine structures volume fraction γ^* are presented in fig. 4. In all the calculations $\gamma^*\sim 0.9$ near the bottom wall, so the solution should be close to the calculation without TCI. In the inviscid core of the flow $\gamma^*\sim 0.5$, at the upper wall upstream from the flame $\gamma^*\sim 0.7$. In these areas TCI is revealed much stronger.

Temperature profiles in three channel cross-sections are given in fig. 5. Upper row of graphs (a) corresponds to the calculations without TCI account and lower row (b) was obtained using PaSR models. The numerical simulations are compared with the experiment and with the calculations from [12] in a similar formulation.

The authors results without TCI account are closer to the experiment than the results of [12]. The temperature overestimation near the lower wall, observed in all sections, is related to inaccurate simulation of heat transport conditions.

In the step vicinity the PaSR models did not improve the calculation accuracy. The curve corresponding to PaSR is shifted away from experimental data. But downstream, at a distance from the step, both PaSR models allowed to noticeably approach the experiment in comparison with calculation without TCI account. For an objective assessment of this improvement, an error of some flow parameter f calculation in each section of the duct was estimated:

$$\varepsilon = \sqrt{\frac{\sum_{i=1}^N (f_i^{\text{comp}} - f_i^{\text{exp}})^2}{N \cdot \max_{i=1, \dots, N} (f_i^{\text{exp}})^2}},$$

where N is the number of experimental points in a given section of the duct. In the flow region with $\gamma^* < 0.7$ the temperature determination error was decreased by 1.8-2.7 times for EPaSR model compared to the calculation without TCI account. The velocity determination error was decreased by 1.7 times for EPaSR. The obtained results are at least not worse than results from [12], obtained in a similar formulation.

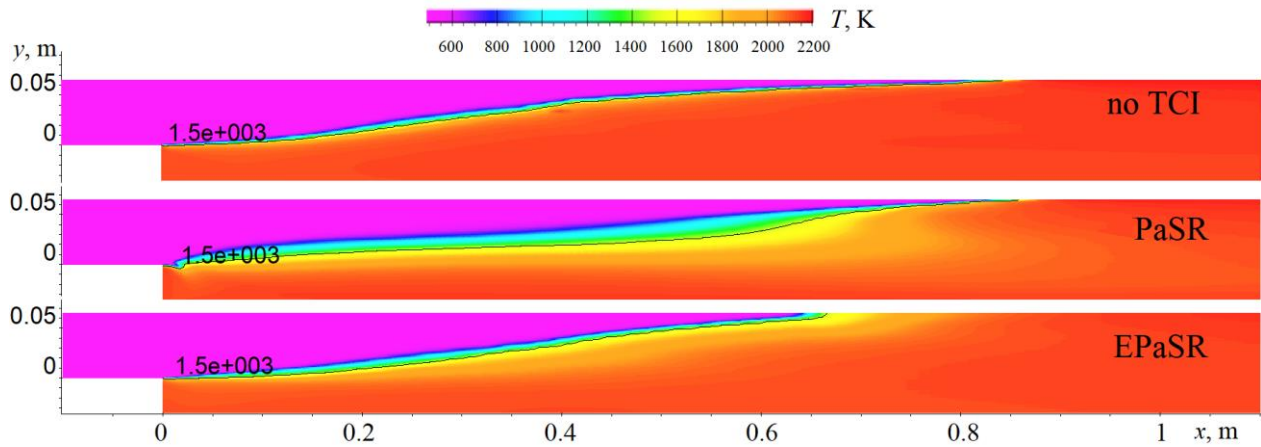


Figure 3: P. Magre et al. [8] experiment modeling: averaged temperature T [K] fields in calculations without TCI account and based on PaSR and EPaSR models

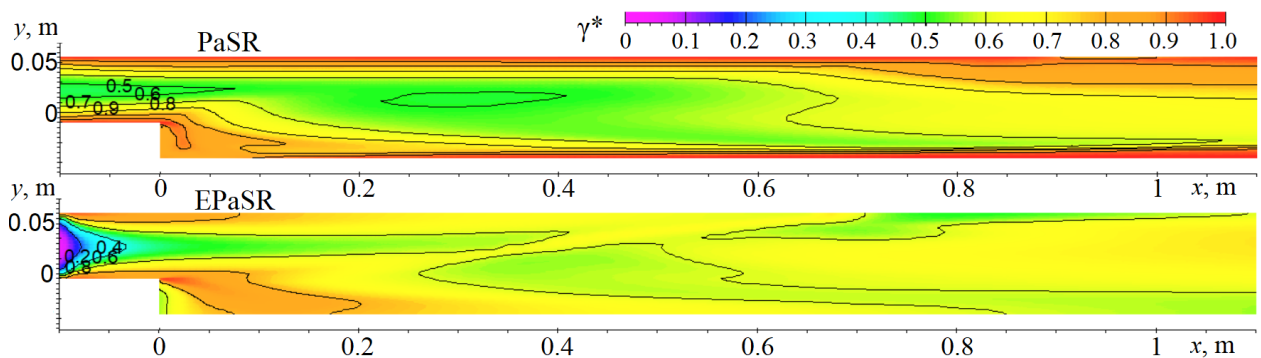


Figure 4: Fine structures volume fraction γ^* in calculations based on PaSR and EPaSR models

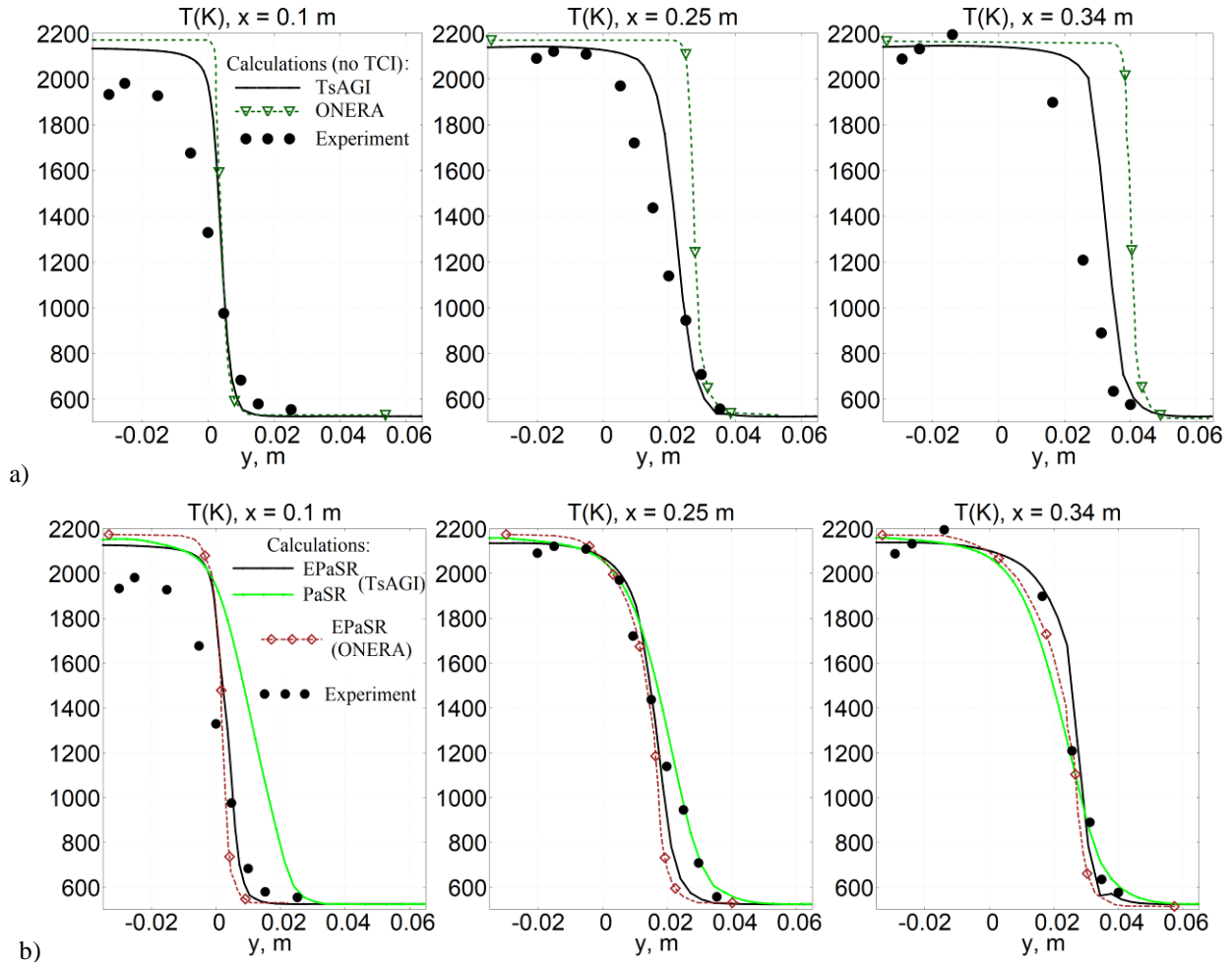


Figure 5: Temperature profiles [K] in sections $x=0.1$ m, $x=0.25$ m and $x=0.34$ m:
 a) calculations without TCI account; b) calculations based on PaSR and EPaSR models

Figure 6 shows the fields of Damköhler $Da = \tau_T / \tau_{chem}$ and Karlovitz numbers $Ka = \tau_{chem} / \tau_K$. At $T = 525$ K, the kinematic viscosity of the mixture is $4 \times 10^{-5} \text{ m}^2/\text{s}$. In our conditions for reactive backward-facing step flow, the laminar flame speed is $S_L \sim 0.9$ m/s and the flame thickness is $\delta_L \sim 5.5 \times 10^{-4}$ m. So the chemical time scale is $\tau_{chem} \sim 6 \times 10^{-6}$ s. The graphs show the distribution of Da and Ka along the flame front. It can be seen that in the region of reactions $Da \gg 1$ and $1 < Ka < 100$. Consequently, one can conclude that this is a regime of thickened flame, where small eddies of the turbulence disturb the internal structure of the flame, causing its thickening. It justifies the applicability of PaSR class models for this flow.

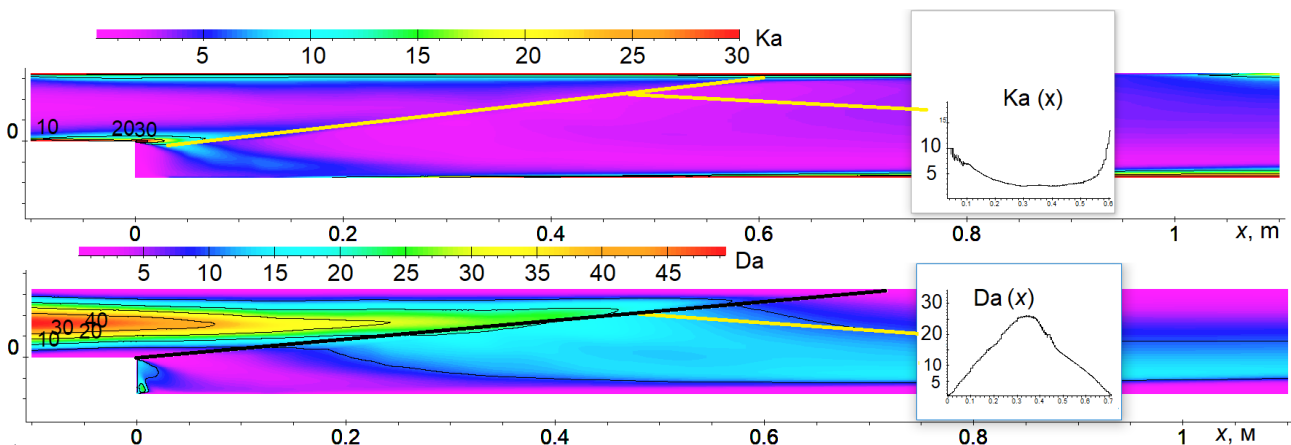


Figure 6: Damkhöler (Da) and Karlovitz (Ka) numbers in the calculations

3.2 Flame stabilization mechanism in P. Magre et al. experiment

In an earlier paper by the authors [15], an attempt was made to explain the flame stabilization mechanism obtained in the numerical simulation of this experiment. This analysis was based on calculations carried out on the described above coarse mesh without taking heat exchange on the chamber walls into account. Far from the step in the calculations, as in the experiment, the wave mechanism of flame propagation was detected, because almost stationary flow of a uniform mixture is realized. But in the vicinity of step the combustion stabilization mechanism, observed in the calculation, did not correspond to real flow pattern with the wave propagation combustion mechanism. In particular, in the region behind the step ($x < 0.25$ m) the heat release rate in the flame front was approximately an order of magnitude higher than for $x > 0.3$ m. But the slope of the flame front near the step implied a decrease in S_W (if the flame front would be a combustion wave).

In the book by L.N. Khitrin [16] it is stated that a combustion wave can stabilize in the flow only if there is a stationary ignition region (an ignition source or an area, where the full flow velocity equal to S_W is maintained due to device geometry). Hence, in the vicinity of the step, the flame front in the calculations was not a burning wave and in the region of $0.25 < x < 0.3$ m, there was a transition from one way of flame stabilization to another.

One aspect obtained in our calculations but physically impossible was the flame stabilization in the immediate vicinity of the wall – it was “clinged” to it. On the one hand, it was caused by the lack of heat exchange on the walls (in the experiment the walls were cooled but the measurement data was not enough to set correctly the boundary condition), and on the other hand, with insufficient grid resolution near the step.

In order to estimate approximately the effect of walls cooling, calculations were performed with a given constant temperature on the wall — options $T_w = 1000$ K, 800 K, 600 K were considered. In fig. 7 you can see the temperature profiles obtained in these calculations for the same sections as in fig. 5. Heat transport consideration allowed to improve the flow description near the walls — the profiles became closer to the experimental points. Variation of the wall temperature within the considered range appeared to be not very essential.

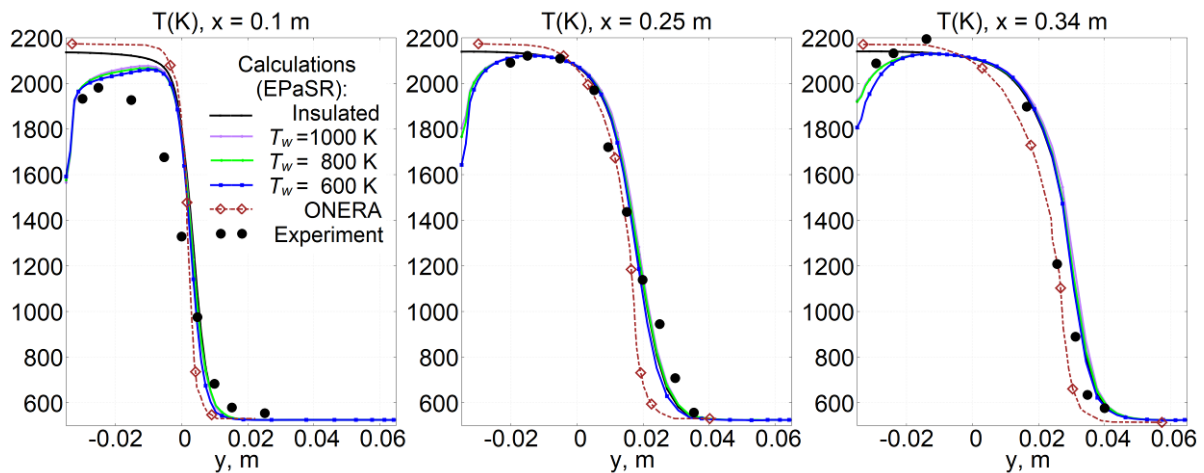


Figure 7: Temperature profiles [K] in sections $x=0.1$ m, $x=0.25$ m and $x=0.34$ m with set wall temperature

For a more detailed description of the flow structure in the step vicinity, calculations were performed on a more detailed mesh (mesh “refst”), which contained an area of size $\Delta x \sim \Delta y \sim h/2$ right and left from the step corner with square cells of the size $\Delta x \sim \Delta y \sim 1.56 \times 10^{-4}$ m (see fig. 8). In total the grid contained about 130 000 cells. It had 134 cells in y direction across the step height and 156 cells across the main stream and 341 cells in x direction along the duct length from the step towards exit. The minimum cells size on the upper wall was $\Delta y \sim 4.25 \times 10^{-4}$ m.

The temperature profiles obtained with EPaSR model on two computational meshes are compared in fig. 9 (the same sections as before are used). Overall, the improved grid resolution did not lead to big changes. Profiles mesh “refst” are closer to the calculations “ONERA” from [12].

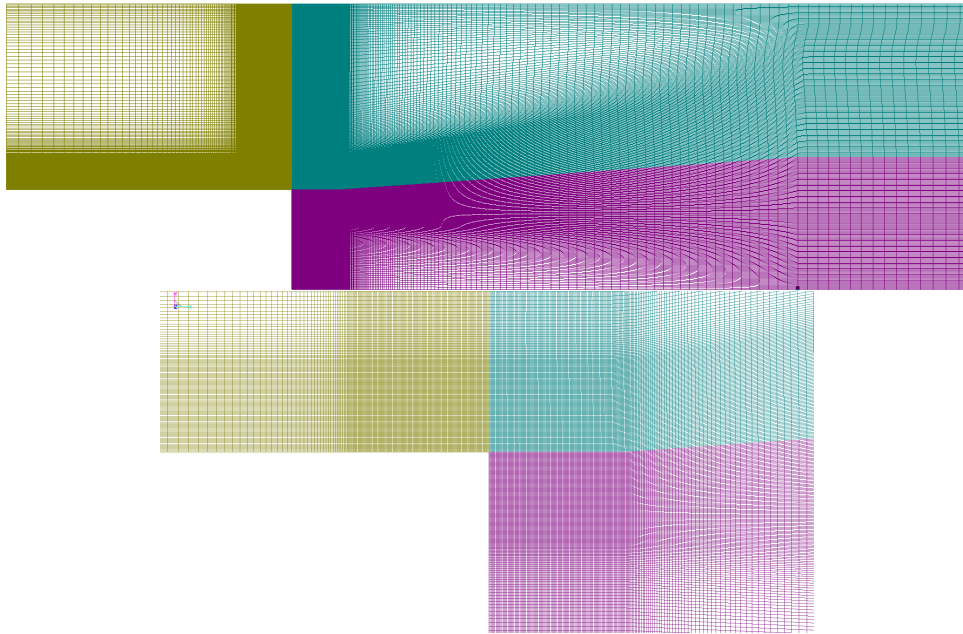
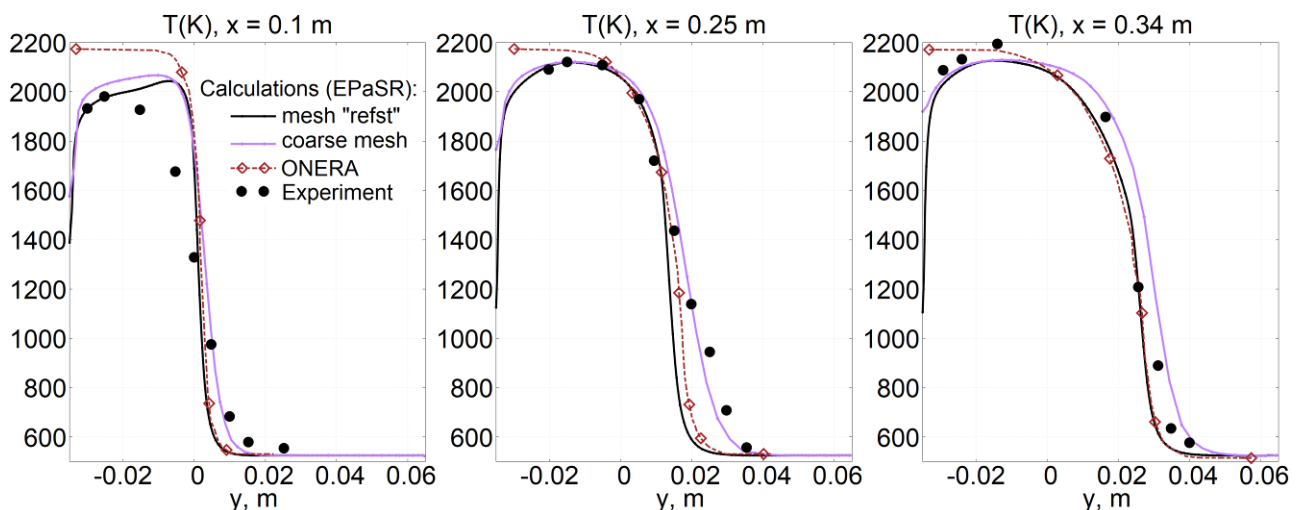


Figure 8: P. Magre et al. [8] experiment modeling: mesh “refst” (general view and mesh in the step vicinity)

Figure 9: Temperature profiles [K] in sections $x=0.1$ m, $x=0.25$ m and $x=0.34$ m: mesh influence

In fig. 10 one can see the decimal logarithm of the rate ϕ of heat release along the streamlines calculated on a “refst” grid with a given wall temperature $T_w=800$ K. It is calculated using the average flow field following the formula [17]:

$$\phi(x, y) = \frac{\sum W_k Q_k}{\rho |\vec{V}|}$$

where Q_k is heat effect of k^{th} reaction [J/mole], ρ – density, and $|\vec{V}|$ is gas velocity. It can be seen that in these calculations the flame does not “cling” to the wall — there is a gap between the wall and beginning of intense heat generation.

Fields of the instantaneous (non-averaged)¹ heat-release rate along streamlines are depicted in fig. 11 a-b for two time moments. It is apparent that there are moments when fresh mixture flows into the recirculation area behind the step (fig. 11, a), and there are moments when the hot burned mixture with the reaction products flows out of this area

¹ Strictly speaking, the use of the formula for ϕ [20] is justified only for a stationary flow, but for a qualitative demonstration it is also reasonable in nonstationary case

(fig. 11, b). Thus, the recirculation region works as a spark plug sustaining combustion in the channel. The flame front position is stationary on average, but periodic oscillations over the mid-position take place. These oscillations are probably related to large eddies arising in the mixing layer because of Kelvin-Helmholtz instability. Naturally, in RANS calculations this process is distorted by eddy viscosity, created by the turbulence model.

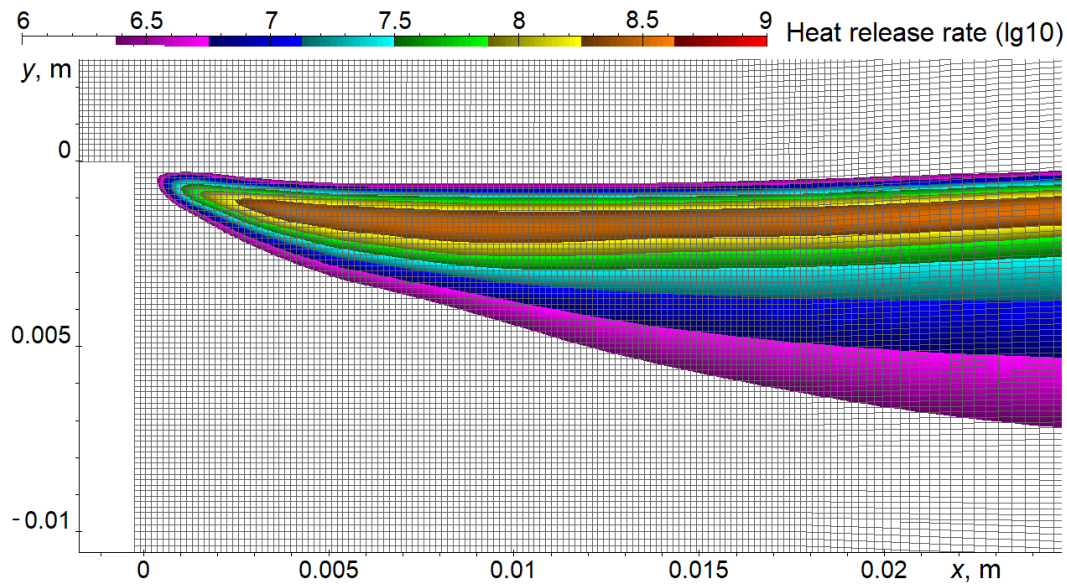


Figure 10: Decimal logarithm of heat release rate along the streamlines ϕ for the average flow field

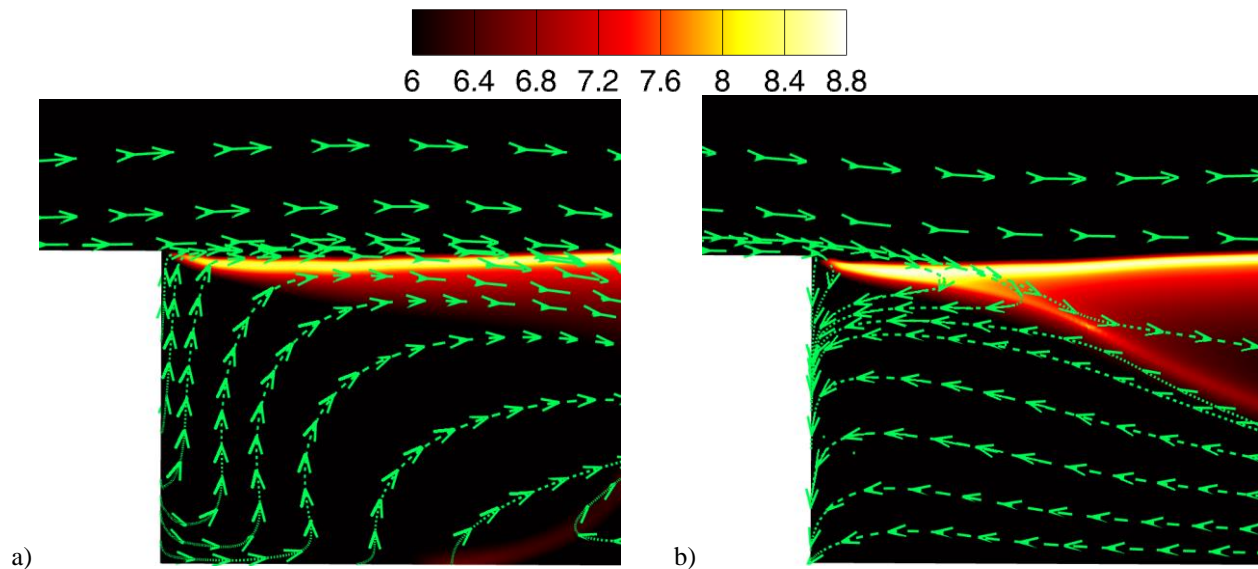


Figure 11: Instantaneous fields of the heat release rate along the streamlines ϕ near the step with velocity vectors at some points: a) fresh mixture inflow and b) hot products outflow

3.3 Flow oscillations in the calculation and mesh convergence of time-averaged field

For a detailed study of fluctuations in the flow, several control points were selected (see fig. 12), where the statistics were gathered. At each time step the values of all gas-dynamic parameters were recorded at these points. In addition, mass flow rate was calculated through the entry and exit sections – G_{entry} and G_{exit} . Time dependencies of these values are shown in fig. 13. Cyclical fluctuations with a period $\Delta t \sim 2.85 \times 10^{-4}$ sec are traced (which corresponds to frequency ~ 3.5 kHz).

Variation of static pressure in the points 1 (near the duct entrance), 2 (near the flame front) and 3 (near the duct exit) is shown in fig. 14. Oscillations with period $\Delta t \sim 2.85 \times 10^{-4}$ sec, related to global oscillations of mass flow rate, may be detected in all three points. However, in points 1 and 2 one may find also oscillations with twice higher frequency. Possible source of these oscillations may be found in fig. 15, where sequential fields of longitudinal velocity are

presented. This figure reveals perturbations, moving along the boundary of separation past the step. This process is repeated after approximately $\Delta t \sim 1.45 \times 10^{-4}$ sec, that corresponds to second frequency in points 1 and 2. It is most probable that these perturbations are resulted from periodical coming of the fresh mixture into the separation that was obvious from fig. 11. These perturbations lead to oscillations of the whole flame front that can be seen in point 2. Pressure oscillations in the point 3 are strongly smoothed because of the grid coarsening towards the duct exit. Additional calculation without chemical reactions has been performed. In that calculation, oscillations have also occurred initially, but finally they damped out. Thus, it is shown that the oscillations are maintained by combustion.

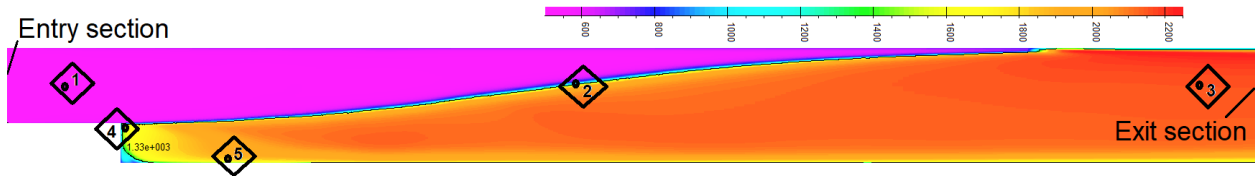


Figure 12: Control points and sections position

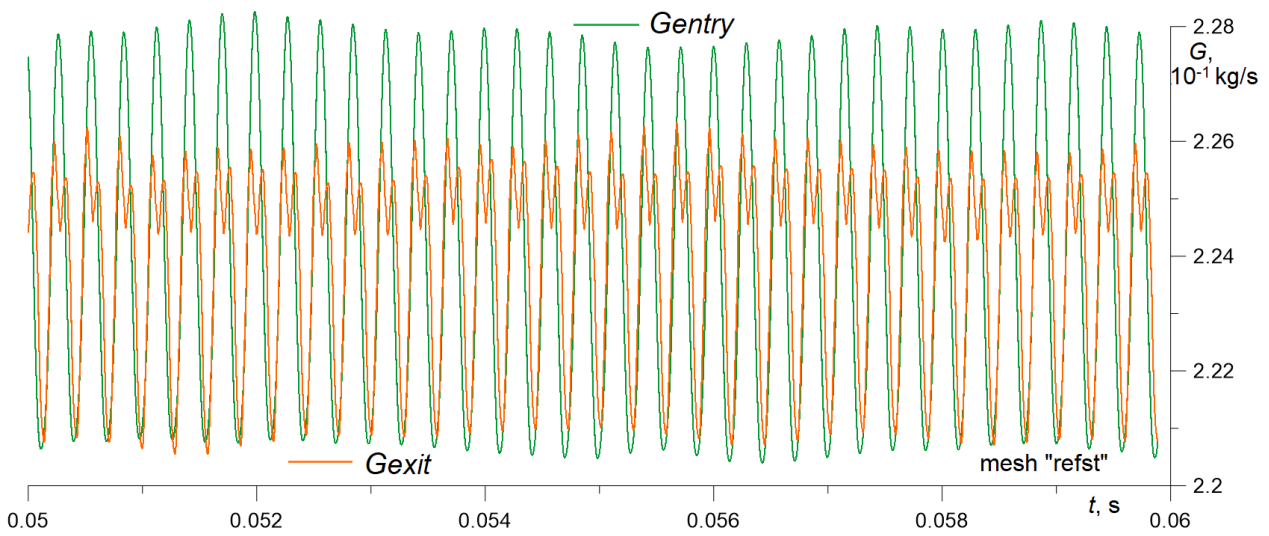


Figure 13: Mass flow rate oscillations (mesh "refst")

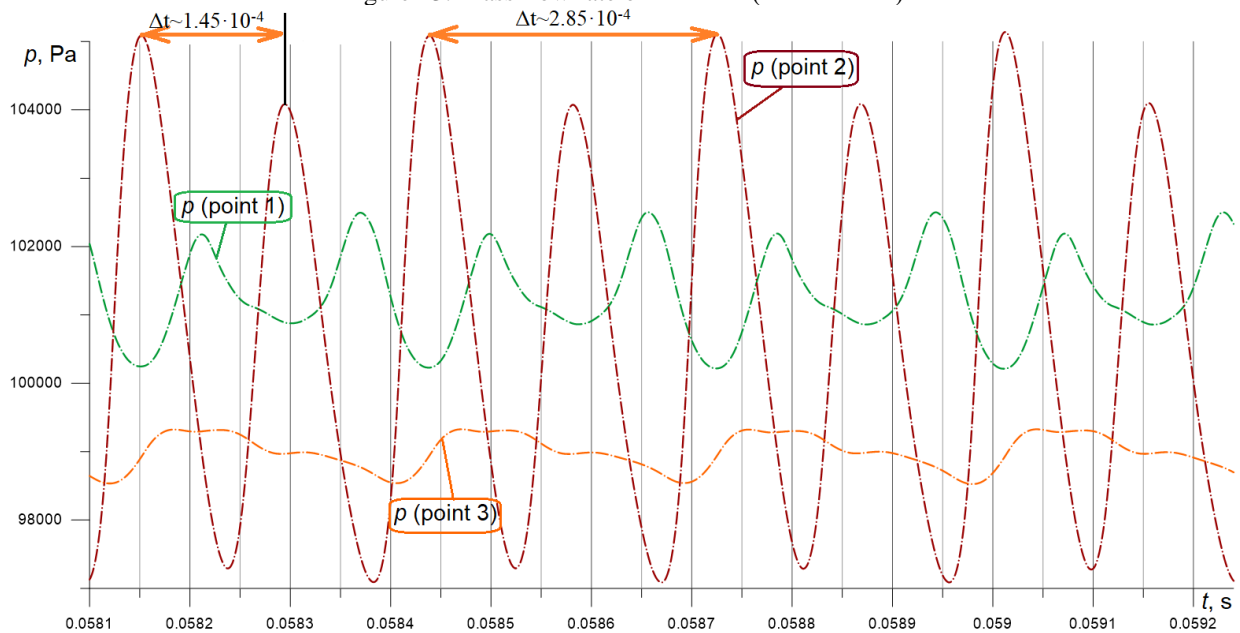


Figure 14: Mesh "refst": oscillations of pressure at control points 1-3

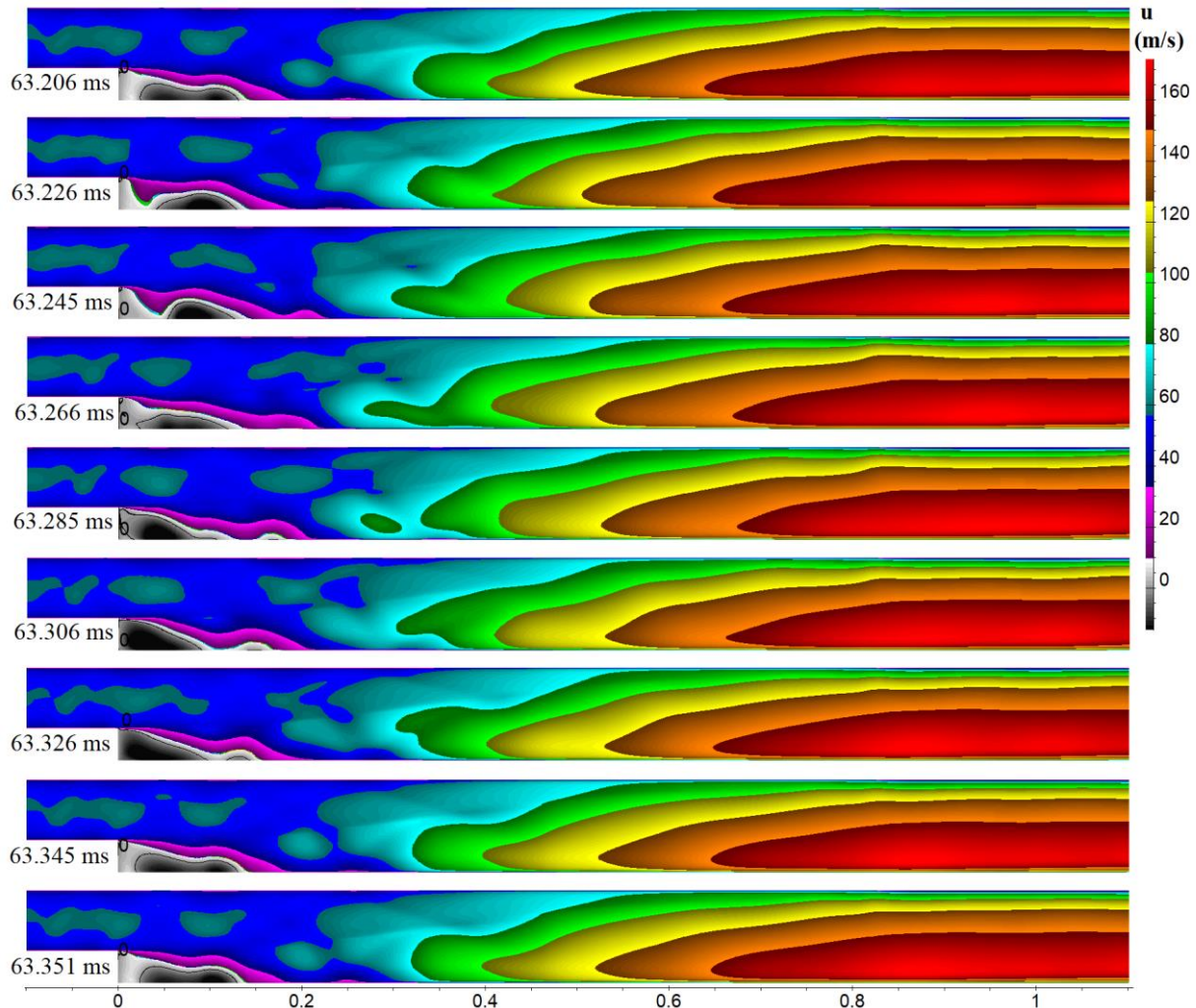
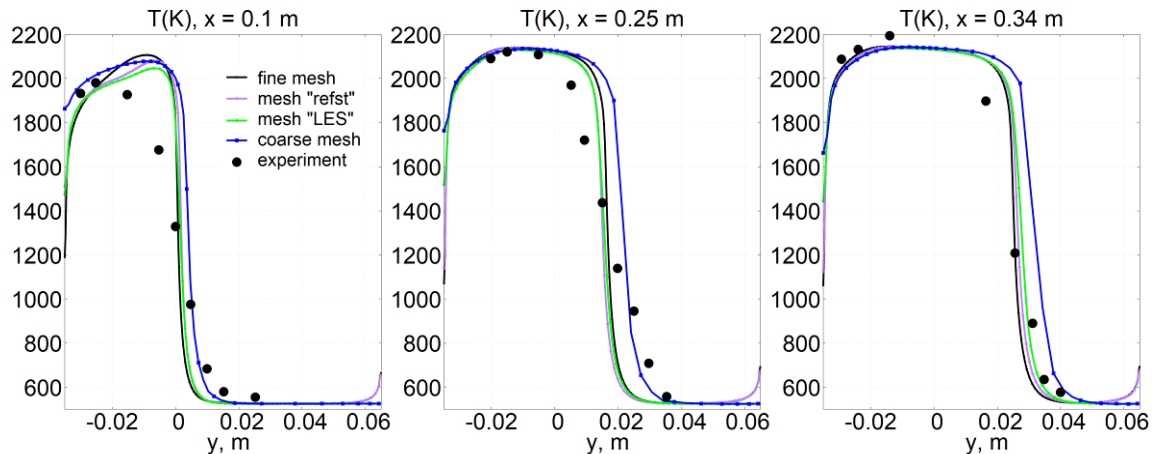


Figure 15: Mesh “refst”: longitudinal velocity fields for several sequential time moments

To study the solution mesh convergence and oscillations mesh dependence, several more computational meshes were considered. For described below LES calculations, a mesh was constructed without refinement to the walls. It contained about 85 000 cells, 208 cells (in y direction) across the step height, 112 higher across the channel height, 1 000 cells in x direction for the channel length. This grid contained almost square cells ($\Delta x \sim \Delta y \sim 3 \times 10^{-4}$ m) behind the step up to $x < 0.1$ m. The mesh step in y direction was constant everywhere. This mesh was better refined in x direction than mesh “refst” in the region $0.05 \text{ m} < x < 0.6 \text{ m}$. RANS calculations were held on this mesh with only one cell in z direction – it will be called “LES” mesh.

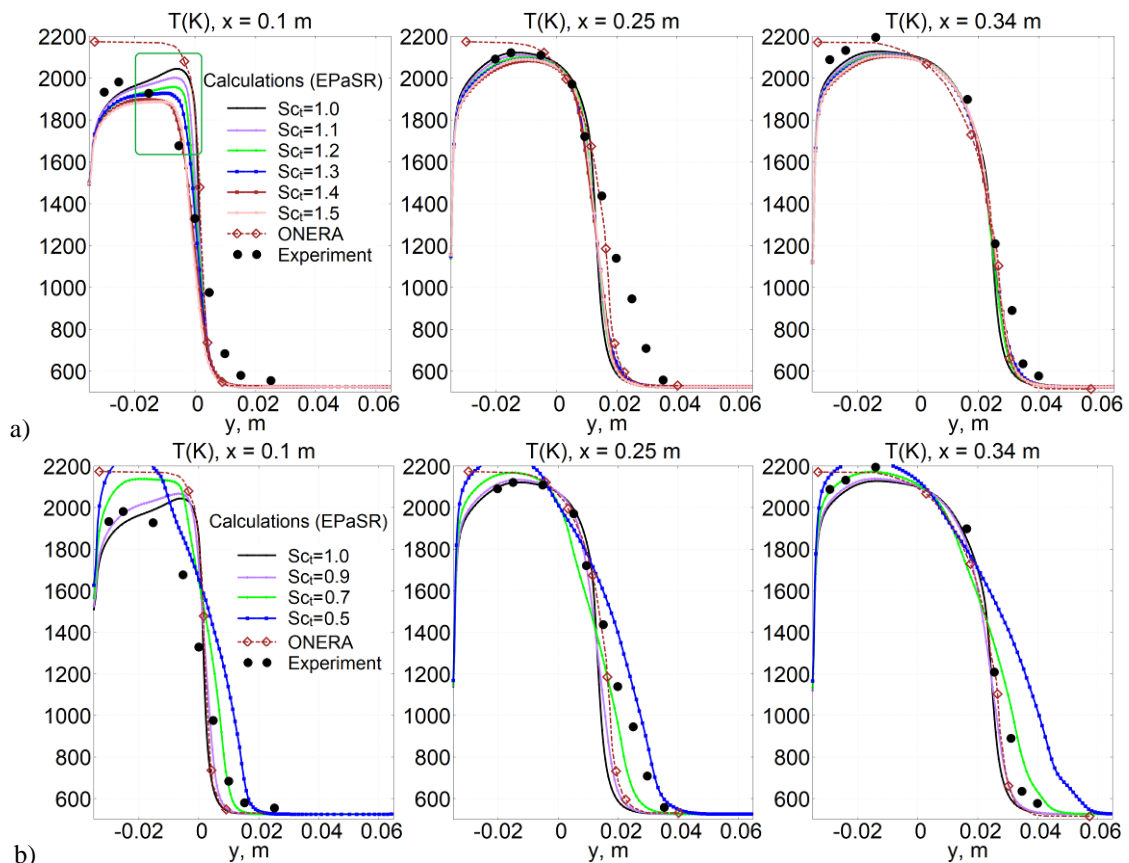
Besides, a detailed fine mesh grid was constructed. It was obtained from mesh “refst” by adaptive refinement and contained about 240 000 cells. This mesh better than the others resolved almost all areas, with the exception of the area $0.26 \text{ m} < x < 0.6 \text{ m}$, where “LES” mesh had smaller x -steps. The detailed fine mesh contains 194 cells across the step height, 156 cells across the channel height and 600 cells for the channel length.

Periodic high-frequency oscillations, analogous to depicted in figs. 13-15, were obtained on every mesh. But the frequency was mesh dependent. The time-averaged solution obtained on each of the meshes differed little from one another. In fig. 16 temperature profiles in the same sections as earlier, obtained in the calculations without TCI are shown. It can be seen that only the curves obtained on the coarsest grid are a little more detached from the rest.

Figure 16: Temperature profiles [K] in sections $x=0.1$ m, $x=0.25$ m and $x=0.34$ m: mesh convergence

3.4 Turbulent transport influence in calculations

So far the authors failed to approach the experiment at a cross section $x=0.1$ m at $0.02 \text{ m} < y < 0$: neither taking TCI into account, not mesh refinement, nor heat transport on the wall description did not affect the flow in this area. Another possible impact tool is turbulent transport description, in particular, turbulent Schmidt number Sc_t adjustment. In order to estimate a possible effect from changes in this parameter, parametric calculations were performed with different but fixed during the whole calculation values of Sc_t . The results of these calculations are shown in fig. 17, a ($Sc_t > 1$) and fig. 17, b ($Sc_t < 1$). It can be seen that turbulent transport description had a noticeable effect on the flow. With $Sc_t=1.3\dots 1.5$ an improvement was achieved in agreement with the experiment in the marked area in fig. 17, a. Reducing the value of $Sc_t < 1$ allowed to get closer to the experimental points in the cross section $x=0.34$ m, worsening the agreement in other sections (fig. 17, b). Probably the use of models with variable turbulent Schmidt number Sc_t values could allow to achieve further improvements in agreement with the experiment.

Figure 17: Temperature profiles [K] in sections $x=0.1$ m, $x=0.25$ m and $x=0.34$ m: a) $Sc_t \geq 1$; b) $Sc_t \leq 1$

3.5 LES calculations

LES calculation of the same configuration and flow conditions was organized. A structured multiblock mesh was used containing 6.8 million cells. It was based on described above mesh “LES” extruded in lateral (z) direction. The computational region occupied a strip $\Delta z=0.05$ m (half of the real lateral width of the chamber), periodic conditions were set on the borders. There were no mesh refinement to the chamber walls; wall functions were used on the boundary. The boundary conditions were set in the same way as in the RANS calculations.

To calculate the convective terms of the equations in eddy-resolving calculations, the upwind WENO5 scheme [18] with the MP monotimizer [19] was used. Time marching was performed with explicit two-step scheme with global time stepping. The IDDES model based on SST [20] was used with shear layer-adapted length scale [21] as a hybrid turbulence model. In-house code zFlare was employed for calculations.

The calculation simulated the time interval $\Delta t=0.06$ s, the flow was allowed to reach statistically stationary flow for 0.02 s and afterwards it was averaged and statistics was collected during 0.04 s. The grid was divided into 128 blocks and same number of HPC cluster processor cores were used. The characteristic calculation time was 1 week. In fig. 18 one can see instantaneous and averaged temperature fields in $z=0$ plane.

The results presented in this paper should be considered as preliminary. At present, averaged temperature profiles are compared with RANS calculations on mesh “LES” and experiment in the same 3 sections as before ($x=0.1, 0.25,$ and 0.34 m) – see fig. 19. As can be seen, the slope angle of the time-averaged flame front in the LES calculation is underestimated. As a result, the discrepancies between LES solution and experiment grow downstream. It will be further studied what improvement can be reached with the thickened flame model [22], low dissipative numerical schemes [23] and considering lateral wall ($z=\text{const}$) boundary layers.

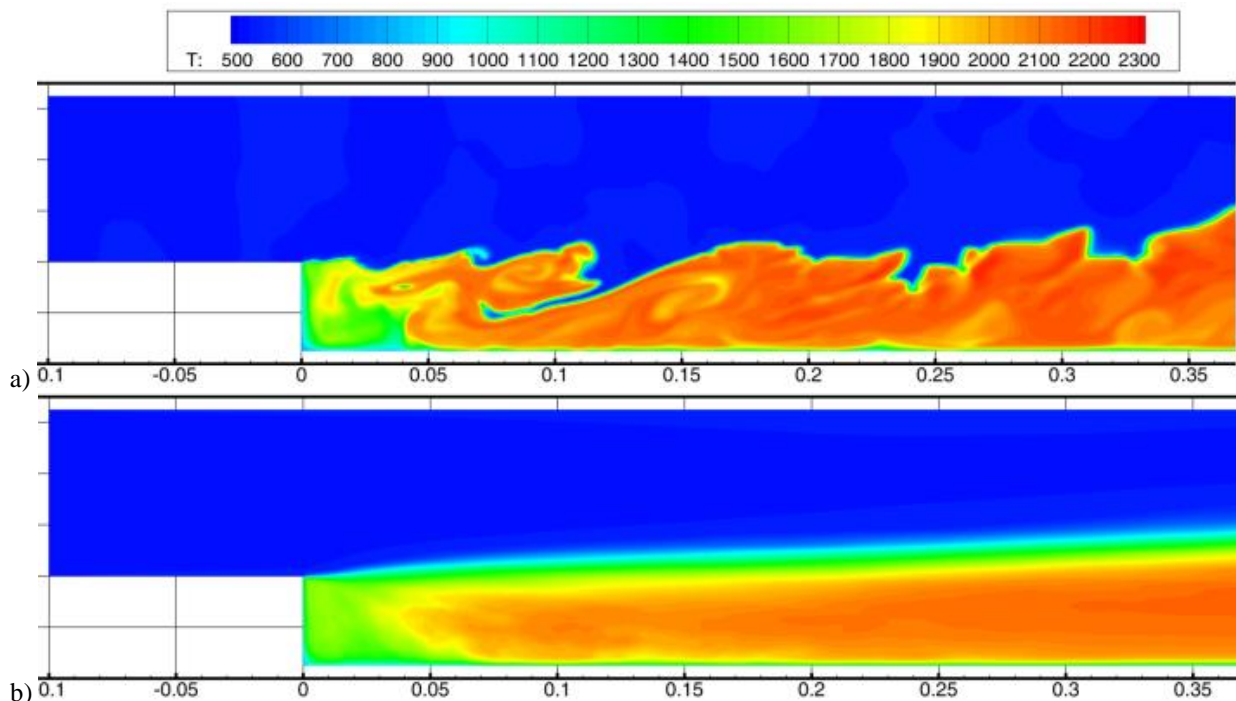


Figure 18: a) Instantaneous and b) averaged temperature fields in LES calculations

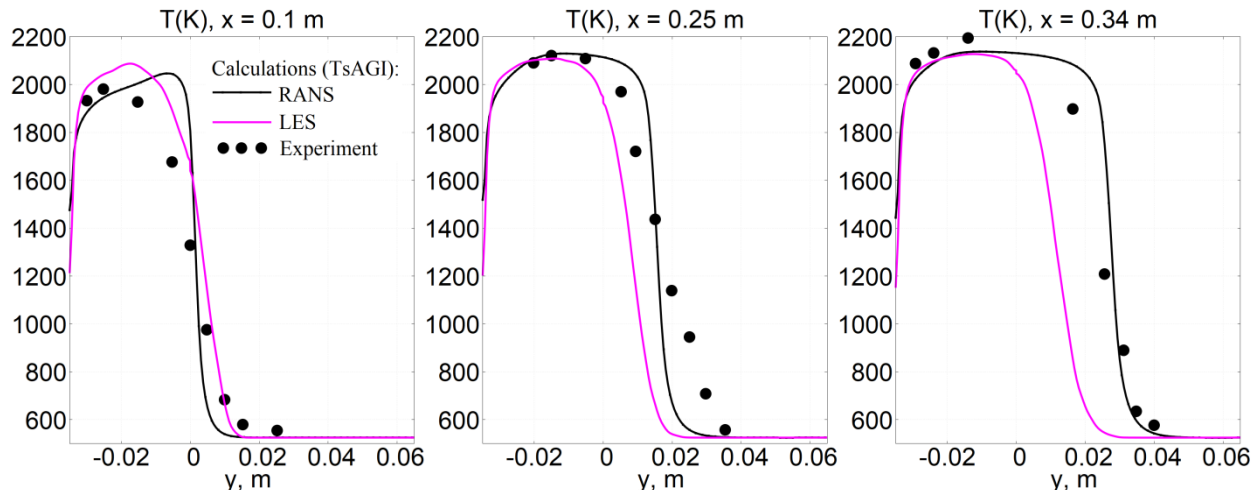


Figure 19: RANS vs LES calculations: temperature profiles [K] in sections $x=0.1$ m, $x=0.25$ m and $x=0.34$ m:

4. Concluding remarks

In simulation of P. Magre et al. experiment the TCI account with EPaSR model allowed to obtain turbulent flame structure and position close to experiment. Improved grid resolution and more accurate consideration of heat transport on channel walls allowed to approach the experiment in flame stabilization mechanism description in the vicinity of the step.

Cyclical fluctuations, related to global oscillations of mass flow rate, were detected in the flow. However, also oscillations with twice higher frequency may be found. It is most probable that these perturbations are resulted from periodical coming of the fresh mixture into the separation. These perturbations lead to oscillations of the whole flame front. It is shown that the oscillations are maintained by combustion.

Turbulent transport description has a noticeable effect on the flow. Considering models with variable turbulent Schmidt and Prandtl numbers remains the task for the future investigations.

The slope angle of the time-averaged flame front in preliminary LES calculation was underestimated. In further LES studied thickened flame model, low dissipative numerical schemes and lateral wall ($z=\text{const}$) boundary layers will be considered.

Acknowledgments

The research was supported by the Ministry of Education and Science of Russian Federation (“megagrant”, agreement No. 14.G39.31.0001).

References

- [1] G. Damköhler. 1940. Der Einfluß der Turbulenz auf die Flammengeschwindigkeit in Gasmischen. *Zeitschrift für Elektrochemie*. 46.
- [2] T. Poinso, D. Veynante. 2005. Theoretical and numerical combustion. 2nd ed. R.T. Edwards, Inc., Philadelphia.
- [3] S.N. Peters. 2000. Turbulent Combustion. Cambridge, UK: Cambridge University Press.
- [4] A.N. Lipatnikov. 2012. Fundamentals of Premixed Turbulent Combustion. Boca Raton, FL: CRC Press.
- [5] Shchetnikov E.S. 1965. Physics of gas combustion. Moscow: “Nauka”.
- [6] V.R. Kuznetsov, V.A. Sabelnikov. 1990. Turbulence and Combustion. Hemisphere, New York.
- [7] S.M. Frolov. 2016. Influence of turbulence on average rate of chemical transformations: review. *Combustion and explosion*. 8(1):215-227.
- [8] P. Magre, P. Moreau, G. Collin, R. Borghi, M. Péalat. 1988. Further studies by CARS of premixed turbulent combustion in a high velocity flow. *Combustion and Flame*. 71(2):147-168.
- [9] V.V. Vlasenko. 2007. About mathematical approach and construction principles of numerical methodologies for applied software package EWT-TsAGI. In a book: “Practical aspects of solving the tasks of the aircraft engine external aerodynamics in the framework of time-averaged Navier-Stokes equations”. *TsAGI Transactions*. 2671:20-85.

-
- [10] A.A. Babulin, S.M. Bosnyakov, V.V. Vlasenko, M.F. Engulatova, S.V. Matyash, S.V. Mikhailov. 2016. Experience of validation and tuning of turbulence models as applied to the problem of boundary layer separation on a finite-width wedge. *Computational Mathematics and Mathematical Physics*. 56(6):1020-1033.
- [11] J. Chomiak, A. Karlsson. 1996. Flame liftoff in diesel sprays. *Symposium (International) on Combustion*. 26(2): 2557–2564.
- [12] N. Petrova. 2015. Turbulence-chemistry interaction models for numerical simulation of aeronautical propulsion systems. PhD Thesis. Ecole Polytechnique.
- [13] Y. Moule, V. Sabel'nikov, A. Mura. 2011. Modelling of self-ignition processes in supersonic non premixed coflowing jets based on a PaSR approach. In: *17th AIAA International Space Planes and Hypersonic Systems and Technologies Conference*. AIAA Paper 2011-2396.
- [14] V.Ya. Basevich, A.A. Belyaev, S.M. Frolov. 1998. "Global" kinetic mechanisms for calculation of turbulent reactive flows. Part 1. The main chemical process of heat release. *Chemical Physics*. 17(9):117-129.
- [15] V.V. Vlasenko, A.Yu. Nozdrachev, V.A. Sabelnikov, A.A. Shiryaeva. 2019. Analysis of the mechanisms of turbulent combustion using calculation data based on the partially stirred reactor model. *Combustion and explosion*. 11(1):43-57.
- [16] L.N. Hitrin. 1957. Physics of combustion and explosion. 452. Moscow University Press.
- [17] V.V. Vlasenko. 2014. About different ways to determine the heat effect and the combustion efficiency in a flow of reactive gas. *TsAGI Science Journal*. 45(1):35-59.
- [18] Zhang R., Zhang M., Shu C.W. 2011. On the order of accuracy and numerical performance of two classes of finite volume WENO schemes. *Communications in Computational Physics*. 9(3):807-827.
- [19] Suresh A., Huynh H. 1997. Accurate Monotonicity-Preserving Schemes with Runge–Kutta Time Stepping. *Journal of Computational Physics*. 136(1):83-99.
- [20] Gritskevich M.S., Garbaruk A.V., Schütze J., Menter F.R. 2011. Development of DDES and IDDES Formulations for the $k-\omega$ Shear Stress Transport Model. *Flow Turbulence Combust.* Springer.
- [21] Shur M.L., Spalart P.R., Strelets M.K., Travin A.K. 2015. An Enhanced Version of DES with Rapid Transition from RANS to LES in Separated Flows. *Flow Turbulence Combust.* 95:709-737. Springer.
- [22] Colin, O., Ducros, F., Veynante, D., and Poinso, T. 2000. A thickened flame model for large eddy simulations of turbulent premixed combustion. *Phys. Fluids*. 12:1843-1863.
- [23] Travin, A., Shur, M., Strelets, M. M., and Spalart, P. R. 2002. Physical and numerical upgrades in the detached-eddy simulation of complex turbulent flows. In: *Advances in LES of complex flows*. 239–254. Springer, Dordrecht.